Journal of Materials Chemistry A

Flux Synthesis of Single Crystal Bismuth Vanadate ($BiVO_4$) Nanowires and their Visible Light Driven Photocatalytic Water Oxidation Properties

Journal:	*Journal of Materials Chemistry A*
Manuscript ID	TA-ART-11-2024-008318.R2
Article Type:	Paper
Date Submitted by the Author:	25-Jan-2025
Complete List of Authors:	Xiao, Chengcan; University of California, Department of Chemistry Assavachin, Samutr; University of California, Department of Chemistry Hahn, William; University of California Davis, Department of Materials Science and Engineering Wang, Li; University of California Davis Department of Chemistry van Benthem, Klaus; University of California, Davis, Dept. for chemical Engineering and Materials Science Osterloh, Frank ; University of California Davis, Department of Chemistry

Flux Synthesis of Single Crystal Bismuth Vanadate ($BiVO_4$) Nanowires and their Visible Light Driven Photocatalytic Water Oxidation Properties

Chengcan Xiao, [a] Samutr Assavachin, [a] William Hahn, [b] Li Wang, [a] Klaus van Benthem,[b] Frank E. Osterloh [a,*]

[a] Department of Chemistry, University of California, Davis, California 95616, United States; https://orcid.org/0000-0002-9288-3407; Email: fosterloh@ucdavis.edu

[b] Department of Materials Science and Engineering, University of California, Davis, California 95616, United States

ABSTRACT

Bismuth vanadate ($BiVO_4$) is a well-known visible light active photocatalyst for the oxygen evolution reaction (OER). In this study, single-crystal $BiVO_4$ nanowires were synthesized for the first time. The nanowires are obtained by recrystallization of $BiVO_4$ microparticles from $NaVO_3$ flux in the 550°C – 700°C temperature range. They exhibit an average thickness of 433.4 ± 110.6 nm and lengths exceeding 20 μm. X-ray diffraction and electron microscopy confirm that the nanowires are single crystals of the monoclinic Scheelite structure type with the [010] crystal direction oriented along the principal wire axis. The nanowires have an optical band gap of 2.41 eV and generate a negative surface photovoltage signal under band gap illumination confirming

their n-type character. A nanowire suspension in aqueous ferric nitrate solution generates oxygen under visible light (390 mW/cm²) at a rate of 28.75 µmol/h and with an apparent quantum efficiency of 0.44% at 405 nm. The relatively low photocatalytic activity of the nanowires can be explained with the absence of a facet-induced charge separation mechanism. Indeed, photolabeling experiments with silver (+) and manganese (2+) ions demonstrate that both photoholes and electrons are extracted along the cylindrical nanowire surface. The fiber morphology makes the $BiVO_4$ nanowires uniquely suited for the construction of membranes for solar energy conversion and photocatalysis.

INTRODUCTION

Monoclinic bismuth vanadate ($BiVO_4$) is a popular visible light active photocatalyst for water oxidation. The material benefits from high chemical stability in neutral or acidic solution and a band gap of 2.4 – 2.5 eV[1–4] that enables it to absorb over 10% of the solar spectrum. Photoelectrochemical water oxidation is enabled by a valence band maximum (VBM) of 2.83 V vs RHE [5] and photocarrier lifetimes of around 40 ns.[6–10] However, because the hole diffusion length is only ~70 nm,[1] and the water oxidation kinetics are slow,[9] nanostructuring of the material and the addition of oxygen evolution cocatalysts are required to achieve performance.[11] For example, a NiFe/$BiVO_4$/SnO_2 photoanode recently achieved a remarkable photocurrent density of 5.61 mA/cm^2 at 1.23 V vs. RHE and an IPCE exceeding 90%, as reported by Yang et al in 2021.[12] In 2023, the highest photocurrent density of 6.29 mA/cm^2 at 1.23 V vs. RHE for photoelectrochemical (PEC) water oxidation and a near unity incident-photon-to-current efficiency (IPCE) of 95.8% was attained from a $BiVO_4$/VO_x photoanode reported by Liu et al.[13]

These PEC devices are all based on $BiVO_4$ films, which allow electron extraction through ohmic contacts and applied potentials. On the contrary, solar energy conversion with $BiVO_4$ particles is much less efficient.[14–22] For example, Okunaka et al. reported in 2016, that $BiVO_4$ nanoparticles (~80 nm) supported with tartaric acid ligands allowed O_2 evolution with a quantum efficiency of 1.2% with Fe^{3+} as electron acceptor.[14] Zhao et al. demonstrated an impressive 71% apparent quantum efficiency (AQE) at 365 nm for photocatalytic water oxidation with decahedral $BiVO_4$ crystals in the presence of Fe^{3+}.[20] Here, charge separation is improved by the electron and hole selective {010} and {110} facets of the crystals. After loading with Ir and $FeCoO_x$ co-catalysts these crystals achieved a solar-to-hydrogen conversion efficiency of 0.6% (AQE of 12.3% at 420 nm) when employed as a Z-scheme photocatalyst with ZrO_2/TaON as the hydrogen evolving particles.[18]

In contrast to other particle shapes,[14–24] one-dimensional nanostructures (nanowires) are distinguished because charge transport is improved along the nanowire direction, which offers advantages for integration into devices.[25] However, achieving a $BiVO_4$ nanowire morphology synthetically has proven difficult, and usually requires the use of structure templates,[26,27] or special techniques, such as electrospinning.[28–33] Spontaneous one-dimensional growth is rarely achieved. In one example, Su, J., et al. reported the fabrication of 1 μm tall $BiVO_4$ pyramid arrays on FTO substrates using seed-mediated growth.[34] In a separate instance, $BiVO_4$ nanowires on titanium foil were obtained by hydrothermal reaction of ammonium vanadate, $Bi(NO_3)_3 \cdot 5H_2O$ in the presence of oxalic acid and hexamethylenetetramine.[35,36] However, the nanowires were contaminated with residual V_2O_5.

Here we demonstrate the first flux synthesis of single crystal $BiVO_4$ nanowires ($BiVO_4$ NWs) in the monoclinic Scheelite phase. The nanowires are obtained by recrystallization of monoclinic $BiVO_4$ microcrystals in $NaVO_3$ flux at 700-550°C. Their structure and morphology are observed with powder X-ray diffraction (XRD) and electron microscopy and their optical and semiconducting properties with UV/vis and Surface Photovoltage Spectroscopy. We further describe the photocatalytic oxygen evolution properties of the nanowires under visible light and the photolabeling results to observe electron and hole collecting sites. Overall, this study describes a new method to obtain single crystalline $BiVO_4$ nanowires and potential uses in sustainable energy applications.

RESULTS AND DISCUSSION

The synthesis of $BiVO_4$ nanowires ($BiVO_4$ NWs) was performed in a $NaVO_3$ flux using $BiVO_4$ microparticles as the reagent (1:10 molar ratio of $BiVO_4$:$NaVO_3$). The choice of $NaVO_3$ as the solvent was inspired by W. Eigermann et al., who reported in 1978 the synthesis of elongated yttrium vanadate (YVO_4) microcrystals from $NaVO_3$ melts.[37] $NaVO_3$ has a melting point of 630°C, while $BiVO_4$ has a 940°C melting point, but is known to soften at ~700°C.[38] Therefore, a temperature of 700°C was selected to completely dissolve the $BiVO_4$ precursors in the $NaVO_3$ flux. The initial $BiVO_4$ microparticles were obtained by reaction of Bi_2O_3 and V_2O_5 in 0.5 M HNO_3 as described in the experimental section. The particles are faceted crystals with dimensions in the 0.2 – 1.0 μm regime (SEM in **Figure S1**). The nanowire synthesis is shown in **Figure 1**. First, the $BiVO_4$ was ground together with solid $NaVO_3$ in 1:10 molar ratio and

transferred to a ceramic (porcelain) crucible with a ceramic cover. The mixture was then heated to 120 ℃ at a rate of 5℃/min and held at this temperature for 5 h to remove any residual water. After that, the mixture was heated further to 700℃ at a rate of 5 ℃/min and kept at that temperature for 10 h to completely dissolve the $BiVO_4$. The flux was then cooled slowly from 700 to 550°C at a rate of -1°C /min. Under these conditions, the $BiVO_4$ forms a super-saturated solution and starts to precipitate in the form of nanowires. Growth is expected to stop at ~630°C due to solidification of the molten $NaVO_3$. After cooling to room temperature, a yellow frozen melt is obtained. The crucible containing the solid melt was placed inside of a 100°C 1.0 M aqueous KOH solution with stirring. After 2 h, the $NaVO_3$ is completely dissolved and the nanowire product can be obtained as a yellow solid by centrifugation.

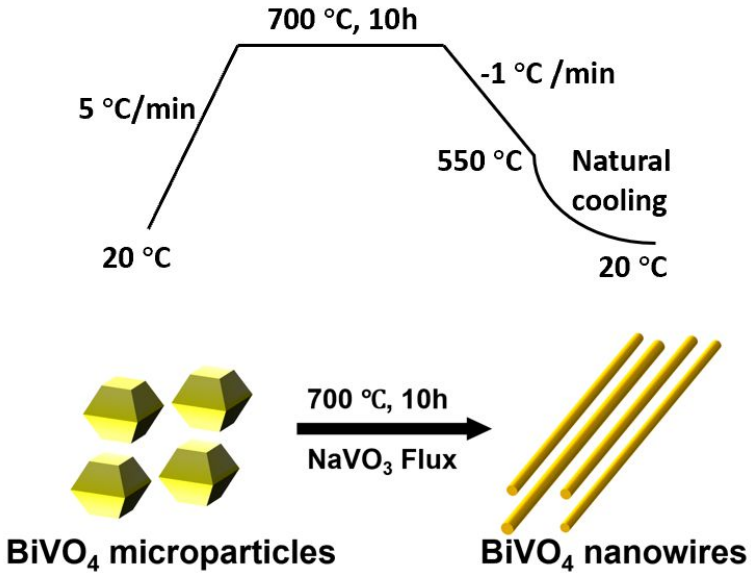

Figure 1. The heating curve and the scheme of the flux-mediated synthesis of $BiVO_4$ nanowires ($BiVO_4$ NWs).

According to SEM (**Figure 2**) the product is composed of nanowires with lengths exceeding 20 μm and with an average diameter of 433.4 ± 110.6 nm. A typical $BiVO_4$ NW (shown in the inset) has a smooth lateral surface and a diameter of 374 nm. The elemental composition of Bi, V, and O was verified by energy dispersive X-ray (EDX) mapping (**Figure 3** and **S3**). Bi, V, and oxygen are found to be clearly associated with the wires, and Bi and V occur in 1:1 atomic ratio within experimental error.

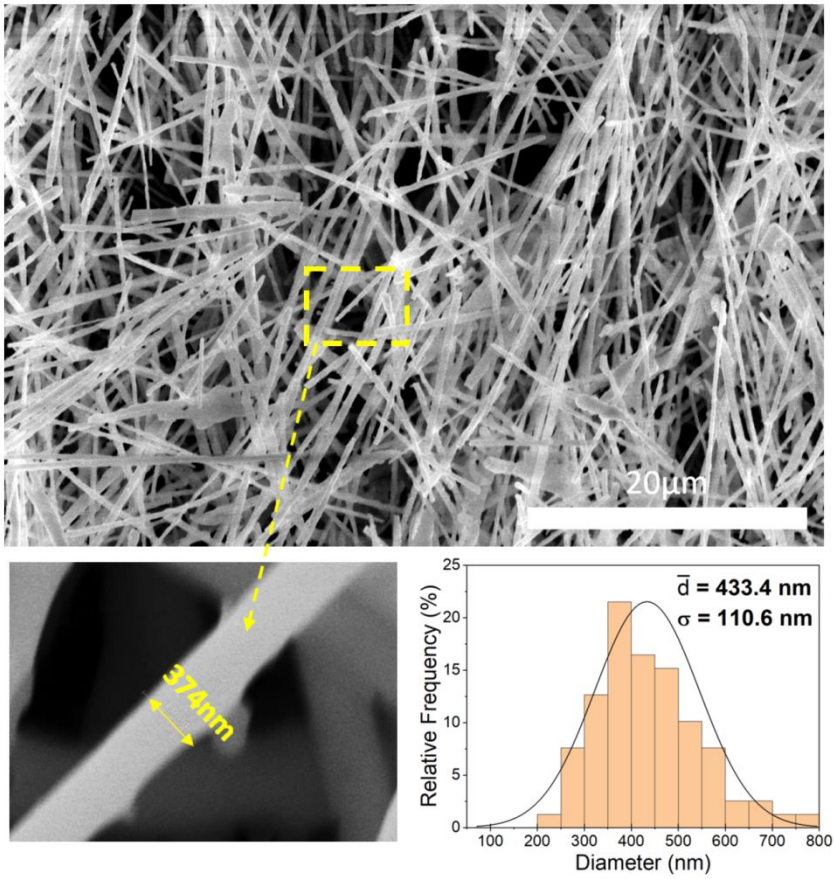

Figure 2. SEM images of the $BiVO_4$ nanowires ($BiVO_4$ NWs). The diameter of a typical nanowire is 374 nm. A distribution of the nanowire diameters is statistically shown in the histogram at the bottom right.

We hypothesize that $BiVO_4$ NWs form by nucleation and anisotropic growth inside the saturated $BiVO_4/NaVO_3$ solution. Therefore, proper adjustment of the $BiVO_4$: $NaVO_3$ molar ratio is very important. For example, only ill-defined $BiVO_4$ crystals are obtained after cooling a solution containing twice the amount of $NaVO_3$ flux solvent ($BiVO_4$:$NaVO_3$ = 1:20 molar ratio, **Figure S2**).

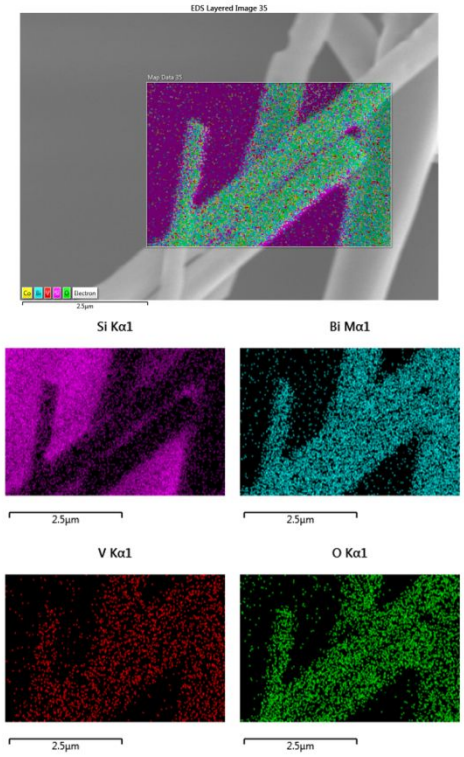

Figure 3. EDX mapping of Bi, V, O, and Si on the $BiVO_4$ nanowires ($BiVO_4$ NWs). The Si signal is from the Si substrate used for the SEM sample.

Powder X-ray diffraction patterns (**Figure 4**) confirm the monoclinic Scheelite crystal structure of the nanowire product.[39] In the diffraction pattern of the $BiVO_4$ NWs, the (040) diffraction peak at 30.6° is significantly intensified compared to the (021) peak, which remains, however, the major peak in the powdered $BiVO_4$ samples. The intensification of the (040) peak indicates that the $BiVO_4$ NWs preferentially grow along the [010] direction.[40] Anisotropic crystal growth is further supported by the intensification of the (020) peak and the decrease of the (200), (20$\bar{2}$), (002), and (40$\bar{2}$) peaks relative to (021).

The location of some facets on a truncated octahedral $BiVO_4$ microparticle is shown in the inset of **Figure 4** to better visualize the growth orientation of $BiVO_4$ NWs from the precursor.

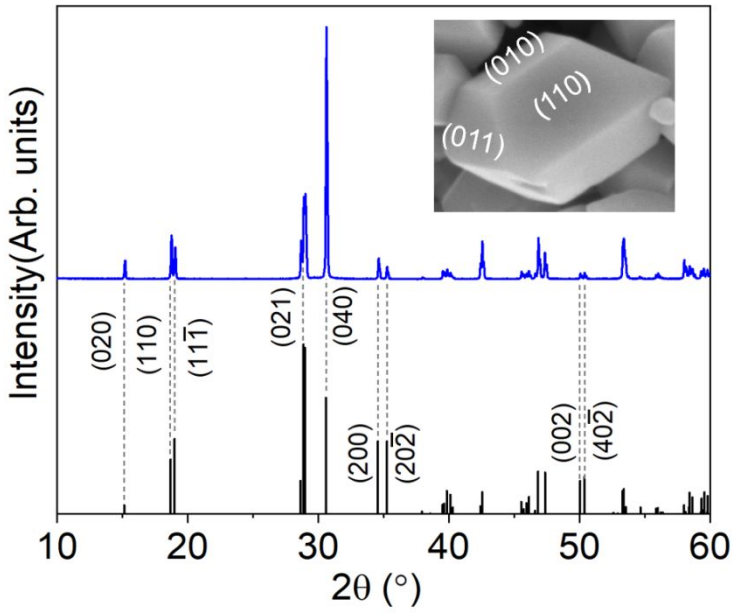

Figure 4. XRD of the $BiVO_4$ NWs confirming the monoclinic Scheelite crystal structure (JCPDS No. 14-0688). The intensified diffraction peak at 30.6° indicates preferential growth of $BiVO_4$ nanowires along the [010] direction. The correlated facets are marked on the SEM inset of a truncated octahedral microparticle.

Transmission electron microscopy (TEM) was employed to examine the microstructure of $BiVO_4$ NWs and to gather local surface information. As can be seen from **Figure 5**, the nanowire appears smooth on the 500 nm scale, but shows small nanospheres on their periphery, which become visible at higher magnification. Using phase contrast imaging lattice fringes of the nanospheres were observed with an interplanar spacing of 0.349 nm, which matches the d_{002}=0.346 nm spacing of (002) planes in α-Bi_2O_3.[41] Therefore, the small particles on the nanowire surface can be attributed to bismuth oxide.

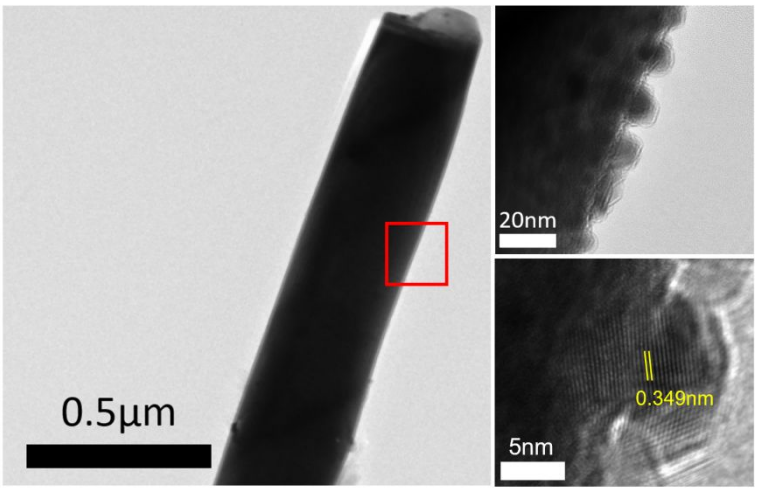

Figure 5. (HR)TEM image (left) and the higher magnification phase contrast images (right) of a $BiVO_4$ nanowire showing approximately spherical shaped nanoparticles at the nanowire surface. A closeup shows lattice fringes of 0.349 nm, which resemble the 0.346 nm d-spacing of (002) facets in alpha-Bi_2O_3.[41]

To dissolve the Bi_2O_3 nanospheres, the nanowires were etched with 1.0 M HNO_3 for ten minutes at room temperature. As shown in **Figure 6**, this treatment removes the spheres from the $BiVO_4$ surface. A selective area electron diffraction (SEAD) pattern recorded for the etched $BiVO_4$ NWs is shown in **Figure 6**. The SAED pattern was recorded in the <001> zone-axis orientation. All spots can be indexed to a single lattice of the monoclinic Scheelite crystal structure. This confirms nanowires are single crystals and grow in the <010> direction.

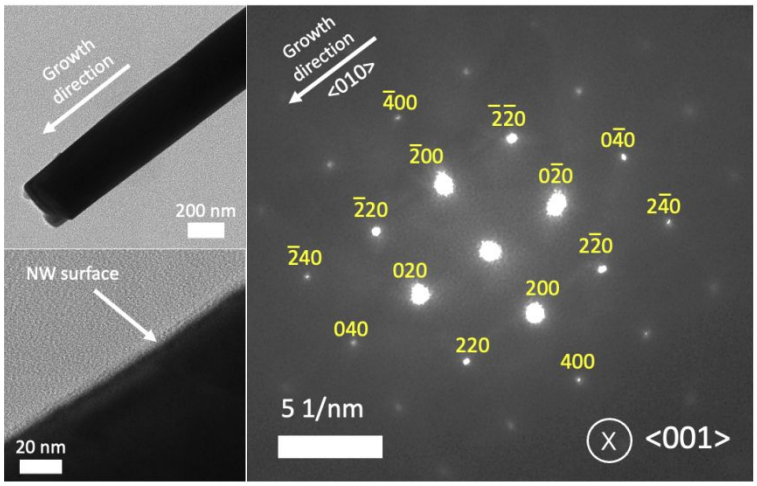

Figure 6. Bright field amplitude contrast HRTEM images and selected area electron diffraction (SAED) pattern of a single $BiVO_4$ nanowire after nitric acid etch. White arrows indicate nanowire growth direction and nanowire surface. Diffraction spots can be indexed to a single lattice of the monoclinic Scheelite structure (JCPDS No. 14-0688).

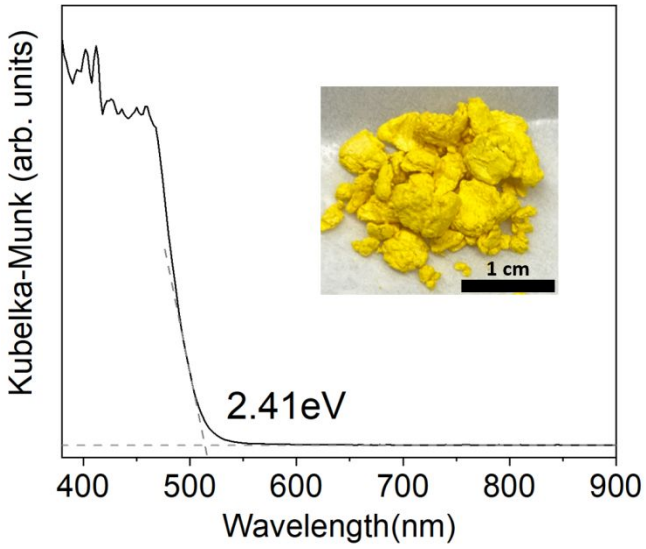

Figure 7. Kubelka-Munk diffuse reflectance spectrum of $BiVO_4$ nanowires ($BiVO_4$ NWs). The inset shows the color of the nanowire aggregates.

A photo and an optical absorption spectrum of the $BiVO_4$ NWs are shown in **Figure 7**. The material forms a cotton-like powder that appears bright yellow. The absorption edge is found at 514 nm, corresponding to an optical bandgap of 2.41 eV. This value matches the reported 2.4 eV bandgap for $BiVO_4$.[42]

To investigate the ability of the $BiVO_4$ NWs to generate a photovoltage under illumination, surface photovoltage spectra (SPS) were recorded on a drop-cast thin film of $BiVO_4$ NWs on a fluorine-doped tin oxide (FTO) substrate. The surface photovoltage signal is plotted in **Figure 8a** versus the photon energy. It is given by the light induced change of the contact potential difference (CPD), SPV=CPD(light)-CPD(dark). The signal is negative, indicative of electron transfer away from the Kelvin probe and towards the FTO. This charge separation direction is controlled by the electric field in the n-type depletion layer as shown in **Figure 8b**. The CPD

onset at 2.25 eV slightly below the 2.41 eV optical bandgap, is attributed to excitation from sub-bandgap defect states such as V^{4+} and O^{-}.[43] The ΔCPD reaches its maximum of -0.46 V at 2.59 eV and returns to the baseline > 4.0 eV due to the diminishing Xe arc lamp intensity at this photon energy. The high photovoltage signal reversibility (88%) suggests minimal hole trapping at the $BiVO_4$ surface.[44] Overall, the SPS spectrum confirms the n-type character of $BiVO_4$ NWs and the presence of defect states near the band edges.

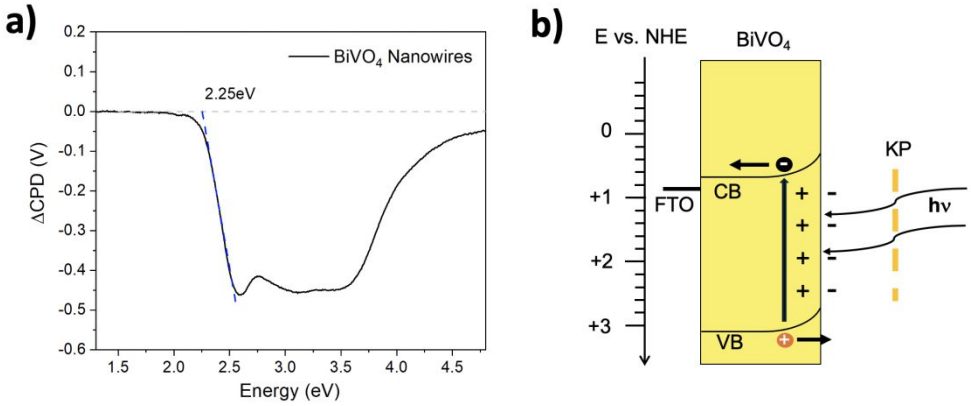

Figure 8. a) Surface photovoltage spectrum (SPS) of $BiVO_4$ nanowire film on FTO in vacuum. b) Schematic energy diagram at pH = 0 showing carrier separation in the space charge region of $BiVO_4$ under illumination. The sample is illuminated through the Kelvin Probe (KP).

To evaluate the photocatalytic activity of the $BiVO_4$ NWs, water oxidation experiments were conducted under visible light (λ > 400 nm) from a 300 W Xe lamp in a round bottom flask containing 100 mg $BiVO_4$ NWs and 100 mL of 0.02 M $Fe(NO_3)_3$. Under these conditions, $Fe(H_2O)_6^{3+}$ serves as an acceptor for photoelectrons from illuminated $BiVO_4$ NWs,[45,46] allowing photoholes to accumulate for water oxidation, as illustrated in the energy diagram in **Figure 9**.

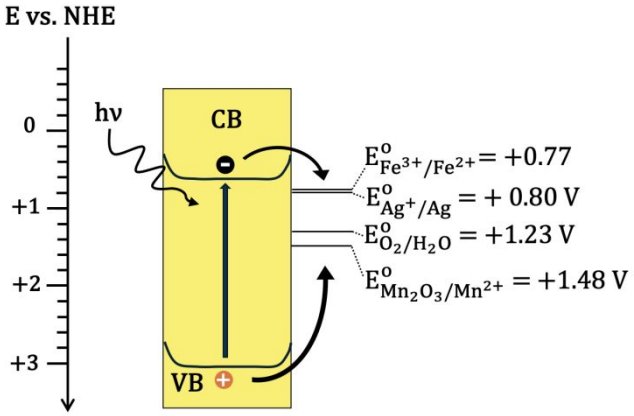

Figure 9. Energy band diagram showing carrier transfer in the gas evolution/photodeposition experiments in $Fe(NO_3)_3$, $AgNO_3$, and $MnCl_2$ solutions under visible light and at pH = 0. The reported conduction band edge of $BiVO_4$ is 0.35 V vs. NHE (4.79 eV vs. vacuum level) and its valence band edge is 2.83 V vs. NHE (7.27 eV vs. vacuum level).[5,47]

As can be seen in **Figure 10a**, the as-prepared $BiVO_4$ NWs evolve some O_2 (black curve) but the rate is very low (2.26 μmol/h). It was hypothesized that this low activity was due to the coverage of surface sites by the Bi_2O_3 nanospheres. Indeed, NWs after 5 min etching with HNO_3 give a much higher O_2 evolution rate (28.75 μmol/h), as indicated by the red curve in **Figure 10a**. This represents a 12.7-fold enhancement, but still is much lower than what is typically observed with $BiVO_4$ particles under such conditions (**Table S1**).[48] Further etching for 10-40 mins in 1.0 M nitric acid did not result in further enhancement, as shown in **Figure S4**. Also, the prolonged etching does lead to surface damage in the form of pits. Some of these pits occur already 5 min into the HNO_3 etch, as can be seen in SEM in **Figure S5**. Lastly, etching of the nanowires with 1.0 M KOH solution was also attempted, but did not result in increased oxygen evolution activity (**Figure S4**).

To investigate the photostability of $BiVO_4$ NWs, a 6 hour continuous gas evolution test was conducted in 100 mL 0.02 M $Fe(NO_3)_3$ solution using a 100 mg sample under Xe lamp irradiation. The visible light intensity at the flask was reduced to 350 mW/cm^2 to slow the consumption of Fe^{3+}, minimizing the impact of Fe^{3+} concentration changes on the oxygen evolution rate of $BiVO_4$ NWs. The flask was evacuated every 2 hours, and the collective oxygen amount was plotted against the reaction time to help evaluate curve linearity, as shown in **Figure S6**. The higher initial oxygen rate is attributed to the release of surface-adsorbed O_2 from the nanowire surface after storage in air. After the first hour, the oxygen evolution rate gradually stabilized, as indicated by improved linearity, but a slow decline in the oxygen evolution rate from consumption of Fe^{3+} and production of Fe^{2+} was still observed. Negligible changes in the optical and morphological properties after the 6 hour test are evidenced by UV-Vis spectra (**Figure S7**) and SEM images (**Figure S8**). These results indicate reasonable photostability of $BiVO_4$ NWs under oxygen evolution conditions.

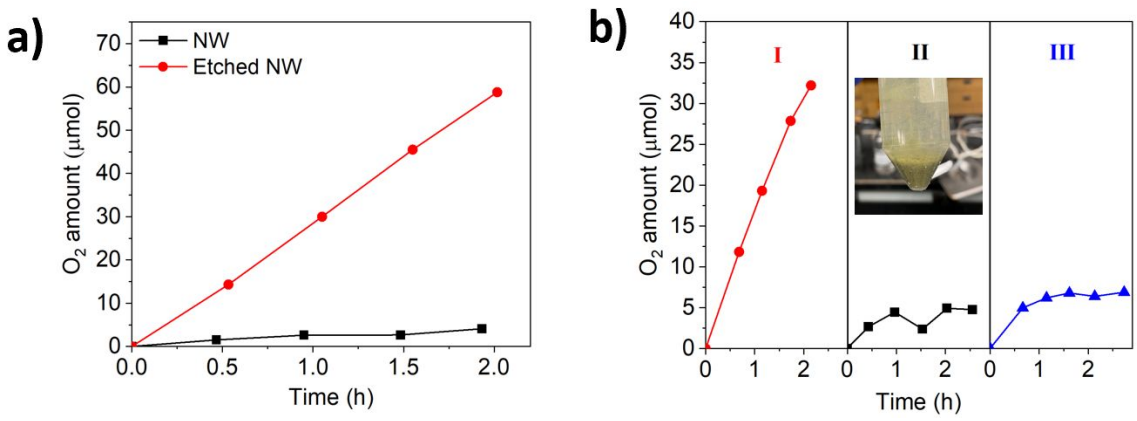

Figure 10. (a) O_2 evolution of 100 mg $BiVO_4$ NWs in 100 mL 0.02 M $Fe(NO_3)_3$ solution under visible light (λ > 400 nm and 32-36° C). (b) O_2 evolution with 5 min etched $BiVO_4$ NWs in 0.02

M $Fe(NO_3)_3$ (I), 0.05 M $AgNO_3$ (II), and mechanically ground $BiVO_4$ NWs in 0.05 M $AgNO_3$ (III). Photo inset: $BiVO_4$ NWs solid after photodeposition of Ag.

Photocatalytic measurements were repeated under the same conditions with the etched $BiVO_4$ NWs and illumination from a 405 nm LED. The corresponding oxygen evolution trace is shown in **Figure S9**. Based on this data, the apparent quantum efficiency of O_2 evolution is 0.44% (Calculation details in the experimental section). For comparison, $BiVO_4$ nanosheets with large (040) and small (200) facets achieved an AQE of 4.5% using Fe^{3+} as the electron scavenger under 440 nm light, as reported by Can Li's group in 2021.[21] The 10 times higher efficiency is attributed to facet induced charge separation, where (040) facets attract photoelectrons and (200) facets attract photoholes. Facet-dependent spatial charge separation is a well-established process for monoclinic $BiVO_4$ microparticles,[19,21,22,49] and also for other photocatalysts, including La:$NaTaO_3$,[50] TiO_2,[51] $SrTiO_3$,[52,53] and WO_3 crystals.[54,55] As recently seen for $SrTiO_3$ single crystals, the facet selectivity is rooted in differences of the facet work functions, and the charge transfer barrier heights of the corresponding semiconductor-liquid junctions.[56]

A simple way to measure the charge selectivity of facets is by photodeposition of Ag, Au, MnO_x, or PbO_2 after reaction of the corresponding metal salts with photogenerated electrons or holes.[19,21] Accordingly, $BiVO_4$ NWs were illuminated in a 0.05 M $AgNO_3$ solution with light from a Xe arc lamp and a 0.22 M $NaNO_2$ UV filter. Because Ag^+ is an effective electron scavenger, O_2 was formed again, as before with $Fe(NO_3)_3$. However, O_2 evolution stopped after 1 hour due to the deposition of silver metal on the nanowires (**Figure 9b**). The optical absorption from Ag also changed the yellow $BiVO_4$ NWs suspension to green (**photo inset**).[57]

According to SEM images and EDX in **Figure 11** and **S10**, most of the Ag grows on the NWs surface and not on the nanowire tips. This shows that photoelectrons are extracted mainly along the NW perimeter.

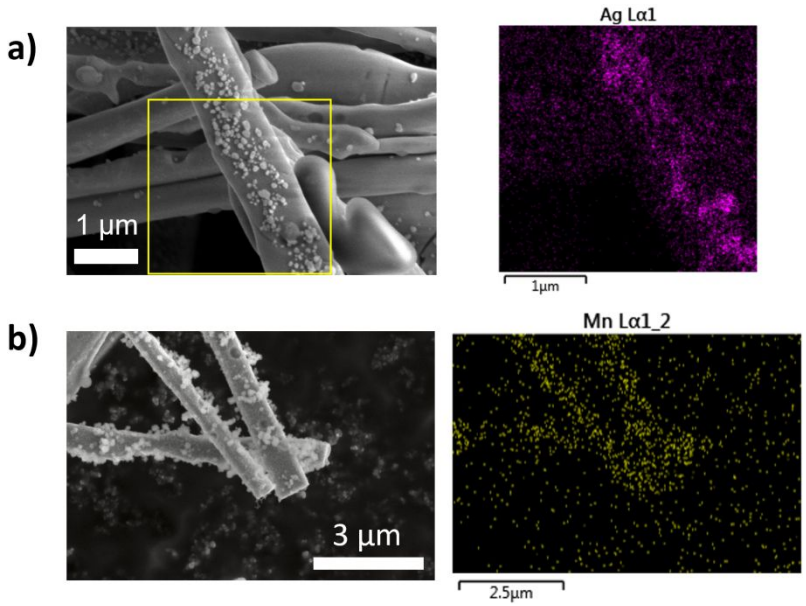

Figure 11. (a) SEM and EDX mapping of Ag at the lateral surface of $BiVO_4$ NWs after photodeposition of Ag. (b) SEM and EDX mapping of Mn at the lateral surface of $BiVO_4$ NWs after photodeposition of MnO_x. Nanoparticles were found on both the lateral and tip surfaces.

In a separate experiment, photohole accumulation sites were identified by photodeposition of MnO_x on $BiVO_4$ NWs from an aqueous solution of 0.02 M $NaIO_3$ and 0.505 mM $MnCl_2$ under >400 nm light from a Xe arc lamp.[19] Here, IO_3^- extracts the photoelectrons while Mn^{2+} captures the photoholes, resulting in the formation of insoluble MnO_x. Inspection of the SEM and EDX data after irradiation for 2 hours (**Figure 11b** and **S11**) reveals MnO_x nanoparticles at both lateral surface and tip surfaces. The Ag and MnO_x photolabeling results demonstrate the

absence of a facet-dependent charge separation mechanism in these $BiVO_4$ NWs. This explains their low quantum efficiency of 0.44% in comparison to other $BiVO_4$ morphologies (**Table S1**). Finally, mechanical grinding was explored to increase the NW tip area composed of (040) facets for potential enhancement in O_2 evolution. However, the same amount of O_2 was generated from photodeposition of Ag (**Figure 9b**). This confirms again that charges are predominantly extracted at the nanowire perimeter, as suggested by the photolabeling results above. An additional factor for the low activity are the large dimensions of the nanowires (average 433 nm diameter and ~20 μm length). These values vastly exceed the electron diffusion length of ~10 nm[58] and hole diffusion length of 45-100 nm[6,8,9,59] in $BiVO_4$, and as a result, photocarriers generated near the nanowire center undergo recombination and cannot be extracted. On the other hand, the measured O_2 evolution rate of 28.75 μmol/h does surpass previously reported rates of 0.075 μmol O_2/h for Ni@NiO-loaded W:$BiVO_4$ nanofibers (NFs)[30] and 13.7 μmol O_2/h for mesoporous undoped $BiVO_4$ NF (see **Table S1**).[28] This is attributed to the single crystal character of the nanowires which suppresses charge recombination and promotes charge transfer. Higher nanowire OER activity may be achievable by adding a water oxidation cocatalyst.

CONCLUSION

In conclusion, we present a scalable synthesis of single-crystalline $BiVO_4$ NWs of monoclinic Scheelite structure type. The NWs have an average diameter of 433 ± 110 nm and lengths exceeding 20 μm. They grow along the [010] direction, based on powder XRD and SAED data. As-grown NWs contain Bi_2O_3 nanocrystals on their surface, which can be removed by etching with 1.0 M HNO_3. The NWs have a 2.41 eV optical bandgap and behave as n-type

semiconductors, based on Surface Photovoltage Spectroscopy. Under visible light, etched $BiVO_4$ NWs evolve O_2 from 0.02 M $Fe(NO_3)_3$ at 28.75 μmol/h, corresponding to an apparent quantum efficiency of 0.44% at 405 nm. The low activity of the material is due to the absence of a facet dependent charge separation mechanism, as confirmed by photodeposition experiments with Ag^+ ion and Mn^{2+} ion. Additionally, the large NW diameter is above the electron and hole diffusion lengths, preventing extraction of short-lived carriers. Improved activity may be achievable with thinner wires and after adding a water oxidation cocatalyst. Thus, the single crystalline nanowires may enable new applications of $BiVO_4$ in photocatalytic membranes (see ref. 27 for example) and overall water splitting devices.

EXPERIMENTAL SECTION

Bi_2O_3 (99.9%, Acros Organics), V_2O_5 (99.6+%, Acros Organics), $NaVO_3$ (96%, Acros Organics), HNO_3 (69.2%, Fisher Scientific), $AgNO_3$ (99+%, ACS reagent, Thermo Scientific Chemicals), $MnCl_2 \cdot 4H_2O$ (99+%, Acros Organics), $Fe(NO_3)_3 \cdot 9H_2O$ (ACS, 98+%, Thermo Scientific Chemicals) porcelain ceramic crucibles (Fisherbrand) were used as received. Water was purified to 18 MΩcm resistivity by a Nano-pure system.

Flux synthesis of $BiVO_4$ nanowires: As the precursor for flux synthesis, $BiVO_4$ microparticles was first synthesized by a liquid-solid state reaction at room temperature and under ambient condition using a procedure reported in the literature.[60] Briefly, 2.33 g Bi_2O_3 and 0.91 g V_2O_5 were mixed in 50 mL of 0.5 M HNO_3 and stirred for 2 days at room temperature. The final product was washed five times in water and left to dry at 70 ℃ in an oven resulting in a yellow powder that was obtained in a yield of 95%.

The as-prepared $BiVO_4$ microparticles were used as the reagent in the flux method with $NaVO_3$ as the flux solvent. 0.648 g $BiVO_4$ was mixed and ground with 2.438 g $NaVO_3$ in 1:10 molar ratio and transferred to a ceramic (porcelain) crucible with a ceramic cover. The mixture of solid salts was heated to 120 ℃ at a rate of 5℃/min and held at that temperature for 5 h to remove any residual water. After that, the mixture was heated to 700℃ at a rate of 5 ℃/min and kept at that temperature for 10 h. Finally, the mixture was cooled to 550 ℃ at a rate of -1 ℃/min and then naturally cooled to room temperature. The resulting yellow solid chunk was immersed in 200 mL of a stirred 1.0 M KOH solution at 100 ℃ for 2 h to remove all $NaVO_3$. The product was separated by centrifugation, washed with 1.0 M KOH once more, and then with water for 4 times, and dried in at 70 ℃ oven overnight. A nitric acid wash was performed on $BiVO_4$ nanowires to remove the surface Bi_2O_3, as well as the oxides from the crucible in some cases. For the acid etch, 40 mg $BiVO_4$ nanowires were dispersed in 10 mL of 1.0 M HNO_3 for 5 mins, 10 min, 20 min and 40 min, followed by washing 3 times with water and drying in a 70 ℃ oven overnight. Base wash in 10 mL of 1.0 M KOH was done by soaking 40 mg of $BiVO_4$ NWs for 10 min or 40 min to study the effect of wash time on their photocatalytic activity.

Photodeposition of Ag and MnO_x as adapted from Li et al[19] with slight modification. Photodeposition of Ag was done in a 100 mL suspension with 100 mg $BiVO_4$ NWs and 0.05 M $AgNO_3$ for 3 hours. Photodeposition of MnO_x was performed in a 50 mL aqueous suspension with 25 mg $BiVO_4$ NWs, 0.02 M $NaIO_3$, and 0.505 mM $MnCl_2$ for 2 hours. The suspensions were sonicated in a 100 mL round bottom flask for 10 min, and the air was then replaced by purging with N_2 for 10 min. Illumination was provided by a 300 W Xe arc lamp equipped with a 0.22 M

$NaNO_2$ long-pass filter (λ>400 nm) and an IR water filter. The irradiance was 400 mW/cm^2 as measured by a GaAsP detector connected to an *International Light* NIST traceable photometer.

Powder X-ray Diffraction scans were conducted with a Bruker D8 ADVANCE Powder Diffractometers, at a wavelength of λ = 0.154 nm. The scan rate was set as 0.14 degree/second.

UV-Vis Diffuse Reflectance Spectroscopy was performed on sample films using a Thermo Scientific Evolution 220 Spectrometer equipped with an integrating sphere. A barium sulfate standard was used to calibrate the background.

Scanning electron microscopy (SEM) images were recorded using the Everhardt-Thornley detector of a FEI Scios instrument operating at of 5.0 keV. Qualitative elemental mapping of the sample was carried out at an acceleration voltage of 20 kV using an Oxford X-Max EDS detector.

Transmission electron microscopy (TEM) was performed with a JEOL 2100F TEM operated at 200 keV. TEM samples were prepared by drop-casting a 0.2 mg/mL suspension of $BiVO_4$ NWs onto carbon supported copper TEM grids, followed by overnight drying at room temperature.

Surface photovoltage spectroscopy (SPS) scans were conducted under vacuum (<1E-4 mbar) using a gold Kelvin probe (Delta PHI Besocke) as the reference electrode. Samples were illuminated with monochromatic light from a 300 W Xe lamp filtered through an Oriel Cornerstone

130 monochromator. NW films were prepared via the following method. First, F-doped tin oxide (FTO) substrates were sonicated sequentially in acetone, ethanol and nano-pure water for 15 min and dried in a 70℃ oven for 2 h before use. Then a 5 mg/mL of $BiVO_4$ NW suspension was prepared and sonicated for 1 h. 50 μL of this suspension was then drop-coated onto a circular area on the FTO substrate as defined by a circular tape mask (diameter = 0.70 cm). The film was dried in air overnight and annealed in air at 400℃ for 2 h. The ramping rate is 2.5℃/min for both heating and cooling.

Photocatalytic water oxidation experiments were conducted in a glass round bottom flask using a mixture of 100 mg $BiVO_4$ nanowires in 100 mL of 0.02 M $Fe(NO_3)_3$ solution. The solution was stirred magnetically and cooled with a fan to 33 ℃ as measured contactlessly with an infrared thermometer. The light from a 300 W Xe-lamp was filtered through a 0.22 M $NaNO_2$ long-pass filter (λ>400 nm) and a water near infrared filter. The visible light intensity at the location of the round bottom flask was ~550 mW/cm^2 as measured by International Light NIST traceable photometer. Prior to illumination, the flask was sonicated for 10 minutes and then connected to an air-tight irradiation setup connected to an SRI GC 8610C gas chromatograph. The 6 hour stability test was performed under the same parameters, except a visible light intensity of ~350 mW/cm^2 was used and vacuum evacuation of the gas space was performed every 2 hours.

Apparent quantum efficiency measurements were conducted as described above in a round bottom flask with magnetic stirring, except a 405 nm LED light source was used, whose light intensity at the flask was 622 mW/cm^2 as measured by an International Light NIST traceable photometer with a GaAsP detector. The back of the flask was covered with an aluminum foil

mirror to reduce photon leakage, leaving an elliptical window of 1.900 cm^2 for the LED. The apparent quantum efficiency (AQE) was obtained with the following equation and values:

$$AQE = \frac{rate\ of\ reacted\ electrons}{rate\ of\ incident\ photons}$$

$$= \frac{micromoles\ of\ O_2\ evolved\ per\ second\ \times 4\frac{electrons}{O_2} \times\ 10^{-6}\ \frac{mole}{micromole}\ \times h\ \times c\ \times F}{P\ \times A\ \times\ \lambda\ \times e}$$

In the above equation, A = 1.900 cm^2 is the area of illumination, P = 622 mW/cm^2 is the light intensity per square centimeter, λ = 405 nm is the wavelength of light, h is the Planck's constant, c is the speed of light, F = 96485 C/mol is the Faraday constant, e is the elemental charge.

SUPPORTING INFORMATION

SEM images, EDX data, oxygen evolution data, quantum efficiency data and a comparison with the reported $BiVO_4$.[14,18,20,21,27,28,30,61–63]

Corresponding Author

Frank Osterloh − Department of Chemistry, University of California, Davis, California 95616, United States; https://orcid.org/0000-0002-9288-3407; Email: fosterloh@ucdavis.edu

Authors

Chengcan Xiao − Department of Chemistry, University of California, Davis, California 95616, United States; https://orcid.org/0000-0001-9664-9338

Samutr Assavachin − Department of Chemistry, University of California, Davis, California 95616, United States; https://orcid.org/0000-0002-6360-3680

William Hahn − Department of Materials Science and Engineering, University of California, Davis, California 95616, United States

Li Wang − Department of Chemistry, University of California, Davis, California 95616, United States;

Klaus van Benthem − Department of Materials Science and Engineering, University of California, Davis, California 95616, United States; https://orcid.org/0000-0001-8865-046X;

Email: benthem@ucdavis.edu

CONFLICTS OF INTEREST

There are no conflicts of interest to declare

ACKNOWLEDGEMENTS

The authors acknowledge the financial support from the National Science Foundation under Grant CHE 1900136. Electron microscopy characterization was carried out at the Center for Nano Micromanufacturing (CNM2) and the Advanced Materials Characterization Laboratory (AMCaT).

REFERENCES

(1) Kim, J. H.; Lee, J. S. Elaborately Modified $BiVO_4$ Photoanodes for Solar Water Splitting. *Adv. Mater.* **2019**, *31* (20), 1806938. https://doi.org/10.1002/adma.201806938.

(2) Wang, S.; Wang, X.; Liu, B.; Guo, Z.; Ostrikov, K. (Ken); Wang, L.; Huang, W. Vacancy Defect Engineering of $BiVO_4$ Photoanodes for Photoelectrochemical Water Splitting. *Nanoscale* **2021**, *13* (43), 17989–18009. https://doi.org/10.1039/D1NR05691C.

(3) Shi, H.; Guo, H.; Wang, S.; Zhang, G.; Hu, Y.; Jiang, W.; Liu, G. Visible Light Photoanode Material for Photoelectrochemical Water Splitting: A Review of Bismuth Vanadate. *Energy Fuels* **2022**, *36* (19), 11404–11427. https://doi.org/10.1021/acs.energyfuels.2c00994.

(4) Kudo, A.; Ueda, K.; Kato, H.; Mikami, I. Photocatalytic O_2 Evolution under Visible Light Irradiation on $BiVO_4$ in Aqueous $AgNO_3$ Solution. *Catal. Lett.* **1998**, *53* (3), 229–230. https://doi.org/10.1023/A:1019034728816.

(5) Cooper, J. K.; Gul, S.; Toma, F. M.; Chen, L.; Glans, P.-A.; Guo, J.; Ager, J. W.; Yano, J.; Sharp, I. D. Electronic Structure of Monoclinic $BiVO_4$. *Chem. Mater.* **2014**, *26* (18), 5365–5373. https://doi.org/10.1021/cm5025074.

(6) Abdi, F. F.; Savenije, T. J.; May, M. M.; Dam, B.; van de Krol, R. The Origin of Slow Carrier Transport in $BiVO_4$ Thin Film Photoanodes: A Time-Resolved Microwave Conductivity Study. *J. Phys. Chem. Lett.* **2013**, *4* (16), 2752–2757. https://doi.org/10.1021/jz4013257.

(7) Ziwritsch, M.; Müller, S.; Hempel, H.; Unold, T.; Abdi, F. F.; van de Krol, R.; Friedrich, D.; Eichberger, R. Direct Time-Resolved Observation of Carrier Trapping and Polaron Conductivity in $BiVO_4$. *ACS Energy Lett.* **2016**, *1* (5), 888–894. https://doi.org/10.1021/acsenergylett.6b00423.

(8) Rettie, A. J. E.; Lee, H. C.; Marshall, L. G.; Lin, J.-F.; Capan, C.; Lindemuth, J.; McCloy, J. S.; Zhou, J.; Bard, A. J.; Mullins, C. B. Combined Charge Carrier Transport and Photoelectrochemical Characterization of $BiVO_4$ Single Crystals: Intrinsic Behavior of a Complex Metal Oxide. *J. Am. Chem. Soc.* **2013**, *135* (30), 11389–11396. https://doi.org/10.1021/ja405550k.

(9) Zhong, D. K.; Choi, S.; Gamelin, D. R. Near-Complete Suppression of Surface Recombination in Solar Photoelectrolysis by "Co-Pi" Catalyst-Modified W:$BiVO_4$. *J. Am. Chem. Soc.* **2011**, *133* (45), 18370–18377. https://doi.org/10.1021/ja207348x.

(10) Rettie, A. J. E.; Chemelewski, W. D.; Emin, D.; Mullins, C. B. Unravelling Small-Polaron Transport in Metal Oxide Photoelectrodes. *J. Phys. Chem. Lett.* **2016**, *7* (3), 471–479. https://doi.org/10.1021/acs.jpclett.5b02143.

(11) Kim, T. W.; Choi, K.-S. Nanoporous $BiVO_4$ Photoanodes with Dual-Layer Oxygen Evolution Catalysts for Solar Water Splitting. *Science* **2014**, *343* (6174), 990–994. https://doi.org/10.1126/science.1246913.

(12) Yang, J. W.; Park, I. J.; Lee, S. A.; Lee, M. G.; Lee, T. H.; Park, H.; Kim, C.; Park, J.; Moon, J.; Kim, J. Y.; Jang, H. W. Near-Complete Charge Separation in Tailored $BiVO_4$-Based Heterostructure Photoanodes toward Artificial Leaf. *Appl. Catal. B Environ.* **2021**, *293*, 120217. https://doi.org/10.1016/j.apcatb.2021.120217.

(13) Liu, B.; Wang, X.; Zhang, Y.; Xu, L.; Wang, T.; Xiao, X.; Wang, S.; Wang, L.; Huang, W. A $BiVO_4$ Photoanode with a VOx Layer Bearing Oxygen Vacancies Offers Improved Charge

Transfer and Oxygen Evolution Kinetics in Photoelectrochemical Water Splitting. *Angew. Chem. Int. Ed.* **2023**, *62* (10), e202217346. https://doi.org/10.1002/anie.202217346.

(14) Okunaka, S.; Tokudome, H.; Hitomi, Y.; Abe, R. Preparation of Fine Particles of Sheelite-Monoclinic Phase $BiVO_4$ via an Aqueous Chelating Method for Efficient Photocatalytic Oxygen Evolution under Visible-Light Irradiation. *J. Mater. Chem. A* **2016**, *4* (10), 3926–3932. https://doi.org/10.1039/C5TA09789D.

(15) Li, G.; Zhang, D.; Yu, J. C. Ordered Mesoporous $BiVO_4$ through Nanocasting: A Superior Visible Light-Driven Photocatalyst. *Chem. Mater.* **2008**, *20* (12), 3983–3992. https://doi.org/10.1021/cm800236z.

(16) Sun, J.; Chen, G.; Wu, J.; Dong, H.; Xiong, G. Bismuth Vanadate Hollow Spheres: Bubble Template Synthesis and Enhanced Photocatalytic Properties for Photodegradation. *Appl. Catal. B Environ.* **2013**, *132–133*, 304–314. https://doi.org/10.1016/j.apcatb.2012.12.002.

(17) Zhao, Y.; Xie, Y.; Zhu, X.; Yan, S.; Wang, S. Surfactant-Free Synthesis of Hyperbranched Monoclinic Bismuth Vanadate and Its Applications in Photocatalysis, Gas Sensing, and Lithium-Ion Batteries. *Chem. – Eur. J.* **2008**, *14* (5), 1601–1606. https://doi.org/10.1002/chem.200701053.

(18) Qi, Y.; Zhang, J.; Kong, Y.; Zhao, Y.; Chen, S.; Li, D.; Liu, W.; Chen, Y.; Xie, T.; Cui, J.; Li, C.; Domen, K.; Zhang, F. Unraveling of Cocatalysts Photodeposited Selectively on Facets of $BiVO_4$ to Boost Solar Water Splitting. *Nat. Commun.* **2022**, *13* (1), 484. https://doi.org/10.1038/s41467-022-28146-6.

(19) Li, R.; Zhang, F.; Wang, D.; Yang, J.; Li, M.; Zhu, J.; Zhou, X.; Han, H.; Li, C. Spatial Separation of Photogenerated Electrons and Holes among {010} and {110} Crystal Facets of $BiVO_4$. *Nat. Commun.* **2013**, *4* (1), 1432. https://doi.org/10.1038/ncomms2401.

(20) Zhao, Y.; Ding, C.; Zhu, J.; Qin, W.; Tao, X.; Fan, F.; Li, R.; Li, C. A Hydrogen Farm Strategy for Scalable Solar Hydrogen Production with Particulate Photocatalysts. *Angew. Chem. Int. Ed.* **2020**, *59* (24), 9653–9658. https://doi.org/10.1002/anie.202001438.

(21) Deng, Y.; Zhou, H.; Zhao, Y.; Yang, B.; Shi, M.; Tao, X.; Yang, S.; Li, R.; Li, C. Spatial Separation of Photogenerated Charges on Well-Defined Bismuth Vanadate Square Nanocrystals. *Small* **2022**, *18* (5), 2103245. https://doi.org/10.1002/smll.202103245.

(22) Xie, Z.; Tan, H. L.; Wu, H.; Amal, R.; Scott, J.; Ng, Y. H. Facet-Dependent Spatial Charge Separation with Rational Cocatalyst Deposition on $BiVO_4$. *Mater. Today Energy* **2022**, *26*, 100986. https://doi.org/10.1016/j.mtener.2022.100986.

(23) Vayssieres, L.; Beermann, N.; Lindquist, S.-E.; Hagfeldt, A. Controlled Aqueous Chemical Growth of Oriented Three-Dimensional Crystalline Nanorod Arrays: Application to Iron(III) Oxides. *Chem. Mater.* **2001**, *13* (2), 233–235. https://doi.org/10.1021/cm001202x.

(24) A. Santori, E.; Iii, J. R. M.; J. Bierman, M.; C. Strandwitz, N.; D. Kelzenberg, M.; S. Brunschwig, B.; A. Atwater, H.; S. Lewis, N. Photoanodic Behavior of Vapor-Liquid-Solid–Grown, Lightly Doped, Crystalline Si Microwire Arrays. *Energy Environ. Sci.* **2012**, *5* (5), 6867–6871. https://doi.org/10.1039/C2EE03468A.

(25) Deng, J.; Su, Y.; Liu, D.; Yang, P.; Liu, B.; Liu, C. Nanowire Photoelectrochemistry. *Chem. Rev.* **2019**, *119* (15), 9221–9259. https://doi.org/10.1021/acs.chemrev.9b00232.

(26) Lei, M.; Liu, J.; Huang, Y.; Dong, Y.; Zhou, S.; Zhao, H.; Wang, Z.; Wu, M.; Lei, Y.; Wang, Z. The Optimization of Optical Modes in Ni-$BiVO_4$ Nanoarrays for Boosting Photoelectrochemical Water Splitting. *Nanotechnology* **2019**, *30* (44), 445403. https://doi.org/10.1088/1361-6528/ab350d.

(27) Liu, B.; Wu, C.-H.; Miao, J.; Yang, P. All Inorganic Semiconductor Nanowire Mesh for Direct Solar Water Splitting. *ACS Nano* **2014**, *8* (11), 11739–11744. https://doi.org/10.1021/nn5051954.

(28) Yu, M.; Shang, C.; Ma, G.; Meng, Q.; Chen, Z.; Jin, M.; Shui, L.; Zhang, Y.; Zhang, Z.; Yuan, M.; Wang, X.; Zhou, G. Synthesis and Characterization of Mesoporous $BiVO_4$ Nanofibers with Enhanced Photocatalytic Water Oxidation Performance. *Appl. Surf. Sci.* **2019**, *481*, 255–261. https://doi.org/10.1016/j.apsusc.2019.03.056.

(29) Wei, J.; Wang, H.; Kang, C.; Ye, X.; Wu, Y.; Liu, B.; Song, C. The Electrospun-Assisted Assembly of Bismuth-Modified $BiVO_4$ Porous Nanofibers with Enhanced Photocatalytic Performance. *New J. Chem.* **2022**, *46* (2), 798–807. https://doi.org/10.1039/D1NJ04862G.

(30) Ro Yoon, K.; Wan Ko, J.; Youn, D.-Y.; Beum Park, C.; Kim, I.-D. Synthesis of Ni-Based Co-Catalyst Functionalized W:$BiVO_4$ Nanofibers for Solar Water Oxidation. *Green Chem.* **2016**, *18* (4), 944–950. https://doi.org/10.1039/C5GC01588J.

(31) Liu, H.; Hou, H.; Gao, F.; Yao, X.; Yang, W. Tailored Fabrication of Thoroughly Mesoporous $BiVO_4$ Nanofibers and Their Visible-Light Photocatalytic Activities. *ACS Appl. Mater. Interfaces* **2016**, *8* (3), 1929–1936. https://doi.org/10.1021/acsami.5b10086.

(32) Cheng, J.; Feng, J.; Pan, W. Enhanced Photocatalytic Activity in Electrospun Bismuth Vanadate Nanofibers with Phase Junction. *ACS Appl. Mater. Interfaces* **2015**, *7* (18), 9638–9644. https://doi.org/10.1021/acsami.5b01305.

(33) Yue, S.; Chen, L.; Zhang, M.; Liu, Z.; Chen, T.; Xie, M.; Cao, Z.; Han, W. Electrostatic Field Enhanced Photocatalytic CO_2 Conversion on $BiVO_4$ Nanowires. *Nano-Micro Lett.* **2021**, *14* (1), 15. https://doi.org/10.1007/s40820-021-00749-6.

(34) Su, J.; Guo, L.; Yoriya, S.; Grimes, C. A. Aqueous Growth of Pyramidal-Shaped $BiVO_4$ Nanowire Arrays and Structural Characterization: Application to Photoelectrochemical Water Splitting. *Cryst. Growth Des.* **2010**, *10* (2), 856–861. https://doi.org/10.1021/cg9012125.

(35) Fang, D.; Cui, M.; Bao, R.; Yi, J.; Luo, Z. In-Situ Coating Polypyrrole on Charged $BiVO_4$ Nanowire Arrays to Improve Lithium-Ion Storage Properties. *Solid State Ion.* **2020**, *346*, 115222. https://doi.org/10.1016/j.ssi.2020.115222.

(36) Fang, D.; Li, X.; Liu, H.; Xu, W.; Jiang, M.; Li, W.; Fan, X. $BiVO_4$-rGO with a Novel Structure on Steel Fabric Used as High-Performance Photocatalysts. *Sci. Rep.* **2017**, *7* (1), 7979. https://doi.org/10.1038/s41598-017-07342-1.

(37) Eigermann, W.; Müller-Vogt, G.; Wendl, W. Solubility Curves in High-Temperature Melts for the Growth of Single Crystals of Rare Earth Vanadates and Phosphates. *Phys. Status Solidi A* **1978**, *49* (1), 145–148. https://doi.org/10.1002/pssa.2210490117.

(38) Dunkle, S. S.; Helmich, R. J.; Suslick, K. S. $BiVO_4$ as a Visible-Light Photocatalyst Prepared by Ultrasonic Spray Pyrolysis. *J. Phys. Chem. C* **2009**, *113* (28), 11980–11983. https://doi.org/10.1021/jp903757x.

(39) Tokunaga, S.; Kato, H.; Kudo, A. Selective Preparation of Monoclinic and Tetragonal $BiVO_4$ with Scheelite Structure and Their Photocatalytic Properties. *Chem. Mater.* **2001**, *13* (12), 4624–4628. https://doi.org/10.1021/cm0103390.

(40) Hu, X.; Masuda, Y.; Ohji, T.; Kato, K. Low-Temperature Fabrication of ZnO Nanoarray Films by Forced Hydrolysis of Anhydrous Zinc Acetate Layer. *J. Cryst. Growth* **2009**, *311* (3), 597–600. https://doi.org/10.1016/j.jcrysgro.2008.09.040.

(41) Malmros, G. The Crystal Structure of Alpha-Bi_2O_3. *Acta Chem. Scand.* **1970**, *24* (2), 384–396.

(42) Kudo, A.; Omori, K.; Kato, H. A Novel Aqueous Process for Preparation of Crystal Form-Controlled and Highly Crystalline $BiVO_4$ Powder from Layered Vanadates at Room Temperature and Its Photocatalytic and Photophysical Properties. *J. Am. Chem. Soc.* **1999**, *121* (49), 11459–11467. https://doi.org/10.1021/ja992541y.

(43) Tan, H. L.; Suyanto, A.; Denko, A. T. D.; Saputera, W. H.; Amal, R.; Osterloh, F. E.; Ng, Y. H. Enhancing the Photoactivity of Faceted $BiVO_4$ via Annealing in Oxygen-Deficient Condition. *Part. Part. Syst. Charact.* **2017**, *34* (4), 1600290. https://doi.org/10.1002/ppsc.201600290.

(44) Daemi, S.; Kundmann, A.; Becker, K.; Cendula, P.; Osterloh, F. E. Contactless Measurement of the Photovoltage in $BiVO_4$ Photoelectrodes. *Energy Environ. Sci.* **2023**, *16* (10), 4530–4538. https://doi.org/10.1039/D3EE02087H.

(45) Suzuki, H.; Kunioku, H.; Higashi, M.; Tomita, O.; Kato, D.; Kageyama, H.; Abe, R. Lead Bismuth Oxyhalides $PbBiO_2X$ (X = Cl, Br) as Visible-Light-Responsive Photocatalysts for Water Oxidation: Role of Lone-Pair Electrons in Valence Band Engineering. *Chem. Mater.* **2018**, *30* (17), 5862–5869. https://doi.org/10.1021/acs.chemmater.8b01385.

(46) Bamwenda, G. R.; Uesigi, T.; Abe, Y.; Sayama, K.; Arakawa, H. The Photocatalytic Oxidation of Water to O_2 over Pure CeO_2, WO_3, and TiO_2 Using Fe^{3+} and Ce^{4+} as Electron Acceptors. *Appl. Catal. Gen.* **2001**, *205* (1), 117–128. https://doi.org/10.1016/S0926-860X(00)00549-4.

(47) Hermans, Y.; Murcia-López, S.; Klein, A.; Krol, R. van de; Andreu, T.; Morante, J. R.; Toupance, T.; Jaegermann, W. Analysis of the Interfacial Characteristics of $BiVO_4$/Metal Oxide Heterostructures and Its Implication on Their Junction Properties. *Phys. Chem. Chem. Phys.* **2019**, *21* (9), 5086–5096. https://doi.org/10.1039/C8CP07483F.

(48) Miseki, Y.; Sayama, K. Highly Efficient Fe(III) Reduction and Solar-Energy Accumulation over a $BiVO_4$ Photocatalyst. *Chem. Commun.* **2018**, *54* (21), 2670–2673. https://doi.org/10.1039/C8CC00257F.

(49) Shen, M.; Kaufman, A. J.; Huang, J.; Price, C.; Boettcher, S. W. Nanoscale Measurements of Charge Transfer at Cocatalyst/Semiconductor Interfaces in $BiVO_4$ Particle Photocatalysts. *Nano Lett.* **2022**, *22* (23), 9493–9499. https://doi.org/10.1021/acs.nanolett.2c03592.

(50) Kato, H.; Asakura, K.; Kudo, A. Highly Efficient Water Splitting into H_2 and O_2 over Lanthanum-Doped $NaTaO_3$ Photocatalysts with High Crystallinity and Surface Nanostructure. *J. Am. Chem. Soc.* **2003**, *125* (10), 3082–3089. https://doi.org/10.1021/ja027751g.

(51) Ohno, T.; Sarukawa, K.; Matsumura, M. Crystal Faces of Rutile and Anatase TiO_2 Particles and Their Roles in Photocatalytic Reactions. *New J. Chem.* **2002**, *26* (9), 1167–1170. https://doi.org/10.1039/B202140D.

(52) Mu, L.; Zeng, B.; Tao, X.; Zhao, Y.; Li, C. Unusual Charge Distribution on the Facet of a $SrTiO_3$ Nanocube under Light Irradiation. *J. Phys. Chem. Lett.* **2019**, *10* (6), 1212–1216. https://doi.org/10.1021/acs.jpclett.9b00243.

(53) Mu, L.; Zhao, Y.; Li, A.; Wang, S.; Wang, Z.; Yang, J.; Wang, Y.; Liu, T.; Chen, R.; Zhu, J.; Fan, F.; Li, R.; Li, C. Enhancing Charge Separation on High Symmetry $SrTiO_3$ Exposed with Anisotropic Facets for Photocatalytic Water Splitting. *Energy Environ. Sci.* **2016**, *9* (7), 2463–2469. https://doi.org/10.1039/C6EE00526H.

(54) Xie, Y. P.; Liu, G.; Yin, L.; Cheng, H.-M. Crystal Facet-Dependent Photocatalytic Oxidation and Reduction Reactivity of Monoclinic WO_3 for Solar Energy Conversion. *J. Mater. Chem.* **2012**, *22* (14), 6746–6751. https://doi.org/10.1039/C2JM16178H.

(55) Liu, G.; Yu, J. C.; Lu, G. Q. (Max); Cheng, H.-M. Crystal Facet Engineering of Semiconductor Photocatalysts: Motivations, Advances and Unique Properties. *Chem. Commun.* **2011**, *47* (24), 6763–6783. https://doi.org/10.1039/C1CC10665A.

(56) Assavachin, S.; Xiao, C.; Becker, K.; Osterloh, F. E. Facets Control Charge Separation during Photoelectrochemical Water Oxidation with Strontium Titanate ($SrTiO_3$) Single Crystals. *Energy Environ. Sci.* **2024**, *17* (10), 3493–3502. https://doi.org/10.1039/D3EE04308H.

(57) Mori, K.; Verma, P.; Hayashi, R.; Fuku, K.; Yamashita, H. Color-Controlled Ag Nanoparticles and Nanorods within Confined Mesopores: Microwave-Assisted Rapid Synthesis and Application in Plasmonic Catalysis under Visible-Light Irradiation. *Chem. – Eur. J.* **2015**, *21* (33), 11885–11893. https://doi.org/10.1002/chem.201501361.

(58) Seabold, J. A.; Zhu, K.; Neale, N. R. Efficient Solar Photoelectrolysis by Nanoporous Mo:$BiVO_4$ through Controlled Electron Transport. *Phys. Chem. Chem. Phys.* **2013**, *16* (3), 1121–1131. https://doi.org/10.1039/C3CP54356K.

(59) Antony, R. P.; Bassi, P. S.; Abdi, F. F.; Chiam, S. Y.; Ren, Y.; Barber, J.; Loo, J. S. C.; Wong, L. H. Electrospun Mo-$BiVO_4$ for Efficient Photoelectrochemical Water Oxidation: Direct Evidence of Improved Hole Diffusion Length and Charge Separation. *Electrochimica Acta* **2016**, *211*, 173–182. https://doi.org/10.1016/j.electacta.2016.06.008.

(60) Iwase, A.; Kato, H.; Kudo, A. A Simple Preparation Method of Visible-Light-Driven $BiVO_4$ Photocatalysts from Oxide Starting Materials (Bi_2O_3 and V_2O_5) and Their Photocatalytic Activities. *J. Sol. Energy Eng.* **2010**, *132* (021106). https://doi.org/10.1115/1.4001172.

(61) Abbood, H. A.; Alabdie, A.; Al-Hawash, A.; Abbood, A. A.; Huang, K. Fabrication of Double-Sided Comb-like F/Ce Co-Doped $BiVO_4$ Micro/Nanostructures for Enhanced Photocatalytic Degradation and Water Oxidation. *J. Nanoparticle Res.* **2020**, *22* (4), 78. https://doi.org/10.1007/s11051-020-04792-z.

(62) He, B.; Li, Z.; Zhao, D.; Liu, H.; Zhong, Y.; Ning, J.; Zhang, Z.; Wang, Y.; Hu, Y. Fabrication of Porous Cu-Doped $BiVO_4$ Nanotubes as Efficient Oxygen-Evolving Photocatalysts. *ACS Appl. Nano Mater.* **2018**, *1* (6), 2589–2599. https://doi.org/10.1021/acsanm.8b00281.

(63) Hu, J.; He, H.; Li, L.; Zhou, X.; Li, Z.; Shen, Q.; Wu, C.; Asiri, A. M.; Zhou, Y.; Zou, Z. Highly Symmetrical, 24-Faceted, Concave $BiVO_4$ Polyhedron Bounded by Multiple High-Index Facets for Prominent Photocatalytic O_2 Evolution under Visible Light. *Chem. Commun.* **2019**, *55* (33), 4777–4780. https://doi.org/10.1039/C9CC01366K.

Data Availability

Data in support of the conclusions of this study is presented in the manuscript and in the Supporting Information section. This data is also available from the corresponding authors upon reasonable request.